ARTICLES
PUBLISHED ONLINE: 9 OCTOBER 2011 | DOI: 10.1038/NPHOTON.2011.255
nature photonics

# Spectral line-by-line pulse shaping of on-chip microresonator frequency combs

Fahmida Ferdous[1], Houxun Miao[2,3]*, Daniel E. Leaird[1], Kartik Srinivasan[2], Jian Wang[1,4], Lei Chen[2], Leo Tom Varghese[1,4] and Andrew M. Weiner[1,4]*

**Recently, on-chip comb generation methods based on nonlinear optical modulation in ultrahigh-quality-factor monolithic microresonators have been demonstrated, where two pump photons are transformed into sideband photons in a four-wave-mixing process mediated by Kerr nonlinearity. Here, we investigate line-by-line pulse shaping of such combs generated in silicon nitride ring resonators. We observe two distinct paths to comb formation that exhibit strikingly different time-domain behaviours. For combs formed as a cascade of sidebands spaced by a single free spectral range that spread from the pump, we are able to compress stably to nearly bandwidth-limited pulses. This indicates high coherence across the spectra and provides new data on the high passive stability of the spectral phase. For combs where the initial sidebands are spaced by multiple free spectral ranges that then fill in to give combs with single free-spectral-range spacing, the time-domain data reveal partially coherent behaviour.**

Optical frequency combs consisting of periodic discrete spectral lines with fixed frequency positions are powerful tools for high-precision frequency metrology, spectroscopy, broadband gas sensing and other applications[1–7]. Frequency combs generated in mode-locked lasers can be self-referenced to have optical frequencies and repetition rates (rates below ~1 GHz in most cases)[8] that are both stabilized. An alternative approach based on strong electro-optic phase modulation of a continuous-wave (c.w.) laser provides higher repetition rates, up to a few tens of gigahertz, but without stabilization of the optical frequency[9–12]. Recently, a novel method for optical frequency comb generation (known as Kerr comb generation) by nonlinear wave mixing in a microresonator has been reported[13–22]. The essential advantages of Kerr comb generation are its simplicity, small size and very high repetition rate.

Most investigations of Kerr combs have emphasized their spectral properties, including optical and radiofrequency (RF) frequency stability. A few experiments have reported time-domain autocorrelation data[23]. Here, we expand the time-domain understanding of these devices by manipulating their temporal behaviour through programmable optical pulse shaping[24]. The large mode spacing of Kerr combs facilitates pulse shaping at the individual line level (also termed optical arbitrary waveform generation, OAWG)[25–29], a technology that offers significant opportunities both in technology (for example, telecommunications, lidar) and ultrafast optical science (for example, coherent control and spectroscopy). We demonstrate line-by-line pulse shaping of microresonator-based frequency combs. An important feature of our approach is that transform-limited pulses may in principle be realized for any spectral phase signature arising from a coherent comb generation process. Furthermore, the ability to achieve successful pulse compression provides new information on the passive stability of the frequency-dependent phase of coherent Kerr combs. Our time-domain experiments also reveal differences in coherence properties associated with different pathways to comb formation.

Figure 1a presents a microscope image of a silicon nitride microring resonator (radius, 40 μm) with a coupling waveguide (described in the Methods). For robust and low-loss coupling of light into and out of the devices, we have developed a process for fibre-pigtailing the chip (Fig. 1b). The fibre-pigtailing used in this device eliminates the time-consuming task of free-space coupling and significantly enhances transportability. Other devices studied make use of a similar V-groove scheme to facilitate coupling alignment, but without a permanent fibre attachment.

Spectroscopy of the optical modes of the resonator was performed using a swept wavelength tunable diode laser with a time-averaged linewidth of less than 5 MHz. Figure 1c shows the transmission spectrum of two orders of transverse-magnetic (TM) modes (with different free spectral range (FSR) and coupling depth), which have their electric field vectors oriented predominantly normal to the plane of the resonator. Figure 1d presents a zoomed-in spectrum for a mode at ~1,556.43 nm with a linewidth of 1.2 pm, corresponding to a loaded optical quality factor ($Q$) of $1.3 \times 10^6$. The average FSR of the series of high-$Q$ modes was measured to be ~4.8 nm. The loaded $Q$-values of the microresonators used in this Article were typically between $1 \times 10^6$ and $3 \times 10^6$.

Figure 2 shows the experimental set-up. The c.w. light was launched into the microresonator, with a polarization controller used to align the input polarization with the TM mode. The generated frequency comb was launched to a line-by-line pulse shaper for spectral phase measurement and correction, which were accomplished simultaneously by optimizing the second harmonic generation (SHG) signal[30,31], as described in the Methods. The pulse shaper was also used to attenuate the pump line, which in our experiments was typically 10–23 dB stronger than the adjacent comb lines, and was sometimes programmed to also attenuate some of the neighbouring lines. This resulted in a spectrum with line-to-line power variations that are reduced (but not completely eliminated), which improves time-domain pulse quality. In ref. 31, the

[1]School of Electrical and Computer Engineering, Purdue University, 465 Northwestern Avenue, West Lafayette, Indiana 47907-2035, USA, [2]Center for Nanoscale Science and Technology, National Institute of Standards and Technology, 100 Bureau Drive, Gaithersburg, Maryland 20899, USA, [3]Maryland Nanocenter, University of Maryland, College Park, Maryland 20742, USA, [4]Birck Nanotechnology Center, Purdue University, 1205 West State Street, West Lafayette, Indiana 47907, USA. *e-mail: amw@purdue.edu; houxun.miao@nist.gov

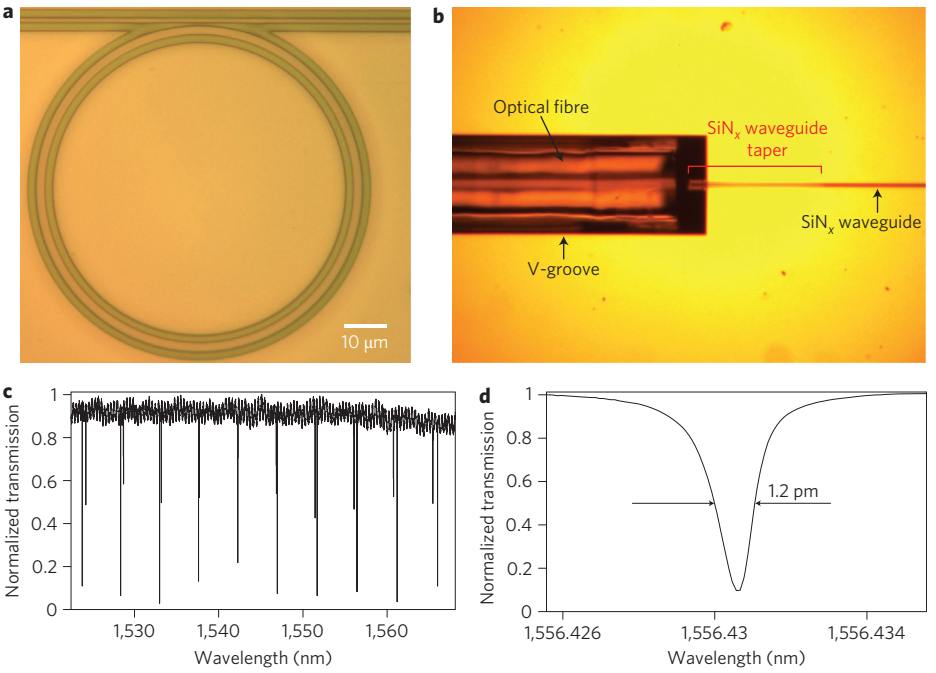


**Figure 1 | High-*Q* silicon nitride microring. a**, Microscope image of a 40-μm-radius microring with a coupling region. **b**, Image of a fibre pigtail. **c**, Transmission spectrum of the microring resonator. **d**, Zoomed-in spectrum of an optical mode with a 1.2 pm linewidth.

phase measurement carried out using this SHG optimization method is compared with another independent method based on spectral shearing interferometry. The difference between the two measurements was comparable to the $\pi/12$ step size of the SHG optimization method. This provides an estimate of both the precision and the accuracy of our phase measurement method. In addition to autocorrelation measurements, which provide information on the temporal intensity, comb spectra were measured both directly after the microresonator and after the pulse shaper and subsequent erbium-doped fibre amplifier (EDFA).

We have investigated comb generation with subsequent line-by-line shaping in a number of devices and have observed two distinct paths to comb formation that exhibit strikingly different time-domain behaviours. Comb spectra measured directly after generation are shown in Fig. 3, with estimated optical powers coupled to the access waveguides given in the figure caption. In some cases, the comb is observed to form as a cascade of sidebands spaced by approximately one FSR, which spread from the pump (Fig. 3a,b,c with comb spacings of ~600, 230 and 115 GHz, respectively). In such cases, which we will refer to as type-I comb formation, high-quality pulse compression has been achieved, indicating good coherence properties. In other cases (Fig. 3d,f), the initial sidebands are spaced by multiple FSRs from the pump. With changes in pump power or wavelength, additional lines spread out from each of these initial sidebands, eventually merging to form a spectrum composed of lines separated by approximately one FSR. For example, Fig. 3d shows a comb comprising nearly 300 lines spaced by 115 GHz; the initial sidebands, which remain evident as strong peaks, are spaced by ~27 FSRs. This route to comb formation, which we will call type-II, has been discussed by several authors[16,17,32,33]. With our devices, type-II formation results in a larger number of lines, but compressibility is degraded in a way that provides clear evidence of partial coherence. Different regimes of comb generation with distinct coherence properties have also recently been reported for combs generated from silica microresonators[34]. Furthermore, variations in comb linewidth under different pumping conditions have also been reported[19].

Figure 4 shows a first set of pulse-shaping results from a microresonator with a radius of 40 μm (Fig. 1a), which generated the type-I comb shown in Fig. 3a, comprising 25 comb lines with a repetition rate of ~600 GHz. The average output power for an estimated 0.45 W coupled into the input waveguide was measured to be 0.10 W. We selected nine comb lines (limited by the bandwidth of the pulse shaper and the bandwidth of the EDFA before the autocorrelator) to perform the line-by-line pulse-shaping experiments. The spectrum after the pulse shaper and the spectral phase profile that was found to maximize the SHG signal are shown in Fig. 4a. Figure 4b shows the measured autocorrelation traces before and after spectral phase correction. The signal appears nearly unmodulated in time without phase correction, but a clear pulse-like signature is present after correction. Such pulse compression clearly demonstrates successful line-by-line pulse shaping. The intensity profile of the compressed pulse, calculated based on the spectrum

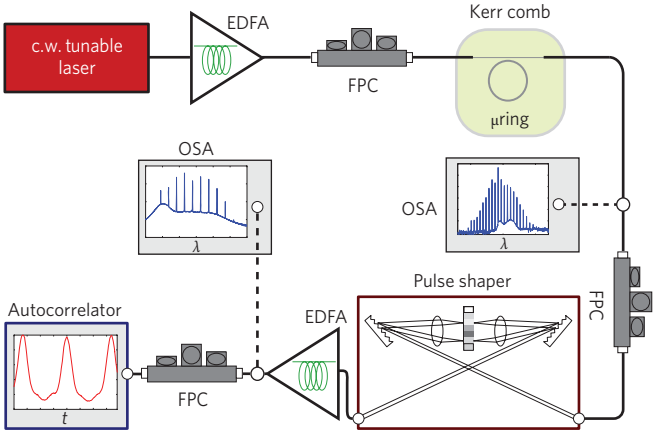


**Figure 2 | Experimental set-up.** Scheme of the experimental set-up for line-by-line pulse shaping of a frequency comb from a silicon nitride microring. FPC, fibre polarization controller; μring, silicon nitride microring; OSA, optical spectrum analyser.

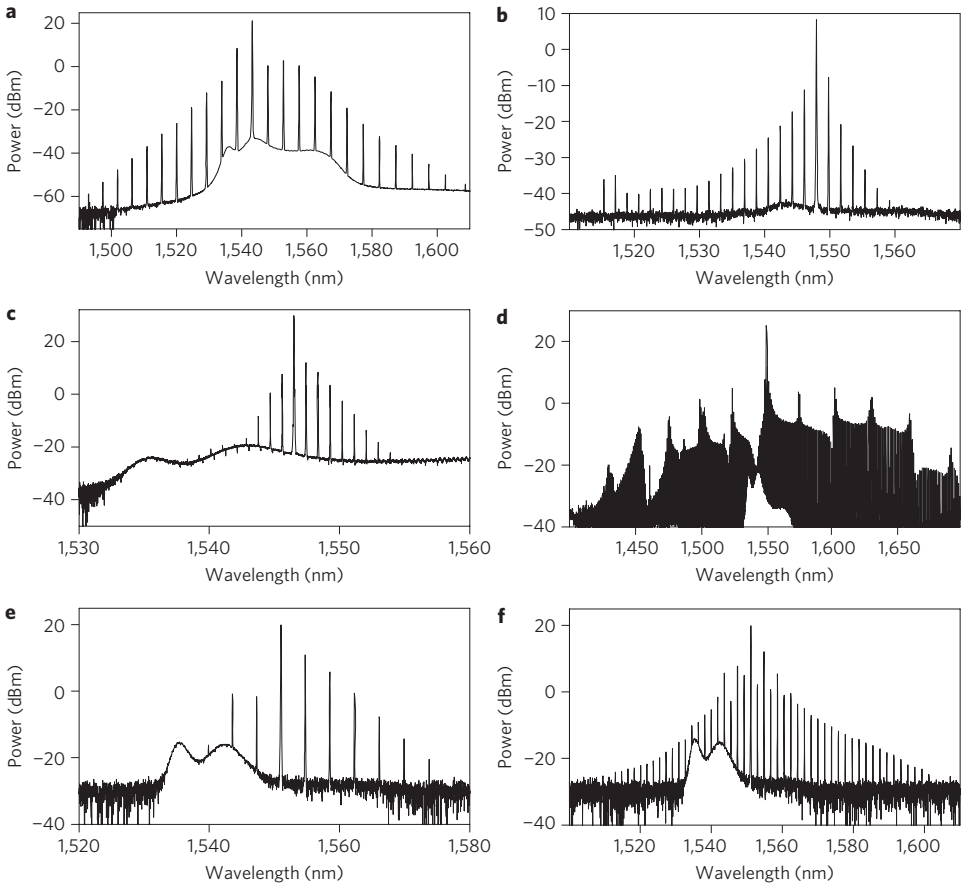


**Figure 3 | Generated Kerr frequency combs from silicon nitride rings. a–f**, Spectra of generated optical frequency combs. For each spectrum, the c.w. pump wavelength, estimated power coupled to the access waveguide, and ring radius are: (**a**) 1,543.07 nm, 0.45 W, 40 μm; (**b**) 1,548.63 nm, 66 mW, 100 μm; (**c**) 1,547.15 nm, 1.4 W, 200 μm; (**d**) 1,549.26 nm, 1.4 W, 200 μm; (**e**) 1,551.67 nm, 1.4 W, 100 μm; (**f**) 1,551.74 nm, 1.4 W, 100 μm.

(Fig. 4a) assuming a flat spectral phase, has a full-width at half-maximum (FWHM) of 312 fs. The corresponding intensity autocorrelation trace was calculated (shown in Fig. 4b) and is in good agreement with the experimental trace. The finite signal level remaining between the autocorrelation peaks arises due to the finite number of lines and the uneven profile of the spectrum. The widths of experimental and computed autocorrelation traces are 460 fs and 427 fs, respectively, a difference of 7%. From this, we take the uncertainty in our 312 fs pulse duration estimation to be $\pm$7%. As a preliminary example of arbitrary waveform generation, we programmed the pulse shaper to apply a $\pi$-step function to the spectrum of the compressed pulse, the results of which are shown in Fig. 4c. The $\pi$ step occurs at pixel number 64 (corresponding to a wavelength of 1,550 nm). Application of a $\pi$-phase step onto half of the spectrum is known to split an original pulse into an electric field waveform that is antisymmetric in time, sometimes termed an odd pulse[35]. The resulting autocorrelation triplet is clearly visible (Fig. 4c), and is in good agreement with the autocorrelation computed based on the spectrum in Fig. 4a and a spectral phase that is flat except for a $\pi$-step centred at 1,550 nm. This result constitutes a clear example of line-by-line pulse shaping for simultaneous compression and waveform shaping.

Similar high-quality pulse compression results have been achieved with other devices exhibiting type-I comb formation. Figure 5 shows data for larger silicon nitride ring resonators (radii, 200 μm and 100 μm), which generate combs spaced by 115 GHz (Fig. 3c) and 230 GHz (Fig. 3b), respectively. These devices have fibre-to-fibre coupling losses as low as 3 dB when lensed fibres are used. The comb spectrum obtained for pumping the 200-μm-radius device at ~1,547 nm exhibits 12 spectral lines, covering a bandwidth of ~10 nm. The comb spectrum obtained for pumping the 100-μm-radius device at ~1,549 nm exhibits 25 spectral lines, covering a bandwidth of ~45 nm (20 spectral lines are left after the shaper). The autocorrelation data again show that although, originally, the signals are at most weakly modulated in time, phase correction results in obvious compression into pulse-like waveforms, yielding autocorrelation FWHM values of 1.78 ps and 976 fs for 200 μm and 100 μm rings, respectively. In both cases, the shape and on–off contrasts of the autocorrelation are in fairly close agreement with the results simulated using the measured spectra and assuming a flat spectral phase.

Time-domain experiments access information about coherence that is not available from frequency-domain data such as the comb spectra. For example, the ability to achieve pulse compression and phase-shaping results as shown in Figs 4 and 5 provides clear evidence of coherence across the comb spectrum. Note that intensity autocorrelation measurements are insensitive both to overall optical phase and to optical phase that varies linearly with frequency. Small changes in pulse repetition rate that would arise from small changes in comb spacing would also be difficult to observe from autocorrelation data (provided that the comb spacing remains uniform across the spectrum). However, autocorrelations do provide information on changes in pulse duration associated with spectral phase variations quadratic or higher in frequency. The close agreement in the shape and on–off contrast of experimental autocorrelation traces, compared with those calculated on the basis of the measured comb spectra (with flat spectral phase), provides evidence that the obtained pulses are not only close to bandwidth-limited, but also

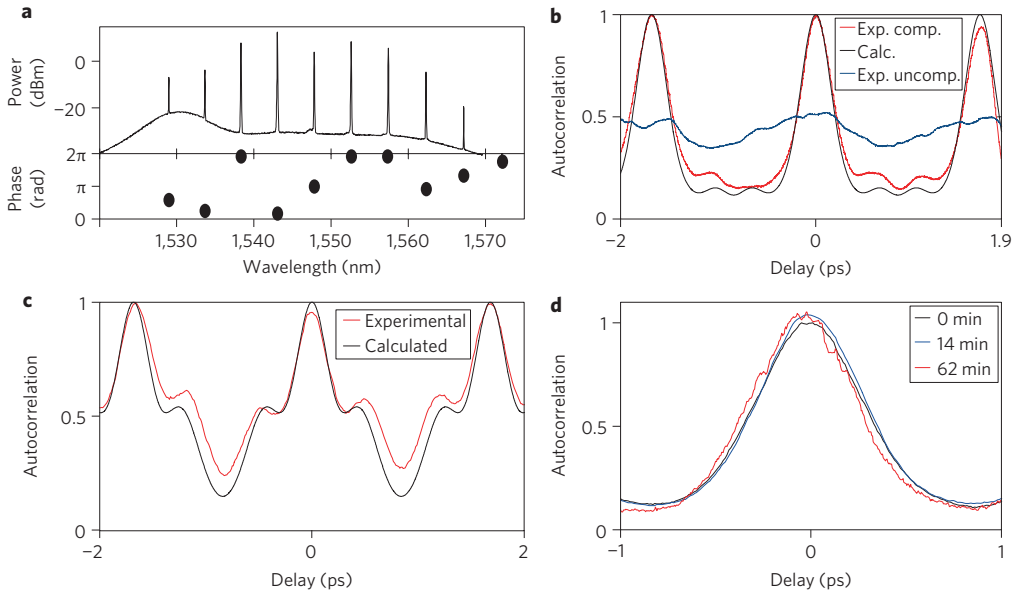


**Figure 4 | Optical arbitrary waveform generation from a Kerr comb. a**, Spectrum of the generated comb (Fig. 3a) after the pulse shaper, as wells as the phase applied to the liquid-crystal modulator pixels of the pulse shaper for optimum SHG. **b**, Autocorrelation traces. Red line, compressed pulse; blue line, uncompressed pulse; black line, calculated by taking the spectrum shown in **a** and assuming a flat spectral phase. The contrast ratio of the autocorrelation measured after phase compensation is 7:1. **c**, The odd pulse: the same phase is applied as in **a**, but with an additional π phase added for pixels 1–64 (wavelengths longer than 1,550 nm). Red line, experimental autocorrelation; black line, autocorrelation calculated using the spectrum of **a**, with a π step centred at 1,550 nm in the spectral phase. **d**, Normalized intensity autocorrelation traces for compressed pulses, measured at 0, 14 and 62 min after spectral phase characterization, respectively.

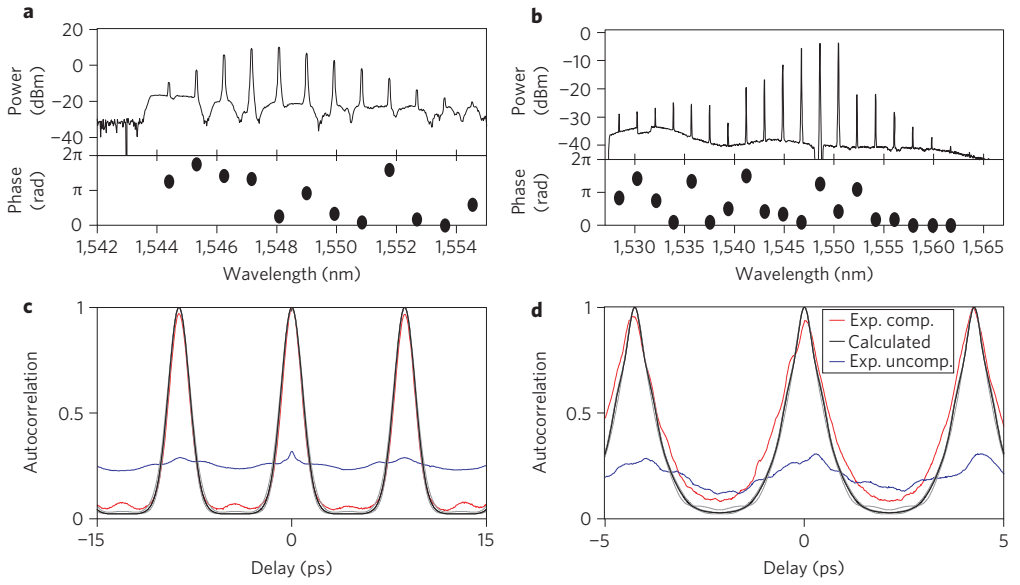


**Figure 5 | Compressed pulses of type-I Kerr combs. a**,**b**, Spectra of the generated combs (corresponding to Fig. 3c and b, respectively) after the pulse shaper, together with the phase applied to the liquid-crystal modulator pixels for optimum SHG signals. **c**,**d**, Autocorrelation traces corresponding to **a** and **b**. Red lines, compressed pulses after phase correction; blue lines, uncompressed pulses; black lines, calculated by taking the spectra shown in **a** and **b** and assuming a flat spectral phase. The contrast ratios of the autocorrelations measured after phase compensation are 14:1 and 12:1, respectively. Light grey traces show the range of simulated autocorrelation traces.

have high coherence. We also observe the autocorrelations over an extended period. Figure 4d shows autocorrelation traces measured at different times within a 62 min interval, with the same spectral phase profile applied by the pulse shaper for all measurements. Clearly the compression results remain similar over the 1 h time period indicated in the figure, which means that the relative average phases of the comb lines must remain approximately fixed; slow drifts in relative average spectral phase must conservatively remain substantially below π. Assume now that the field consists of lines at frequencies $f_o + nf_{rep} + \delta f_n$, where $f_o$ is the carrier-envelope offset frequency, $f_{rep}$ is the repetition rate, and $\delta f_n$ refers to small fixed shifts (assumed to be random and uncorrelated) of

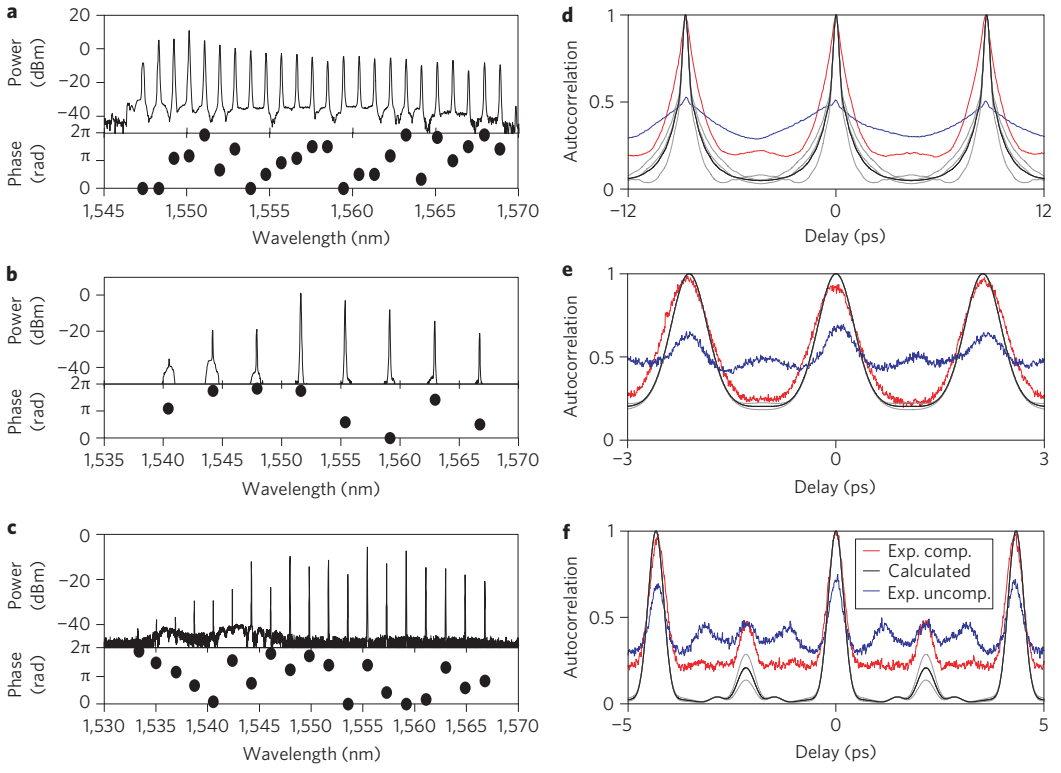


**Figure 6 | Compressed pulses of type-II Kerr combs. a–c**, Spectra of the generated comb (corresponding to Fig. 3d,e,f, respectively) after the pulse shaper, together with the phase applied to the liquid-crystal modulator pixels for optimum SHG signals. **d–f**, Autocorrelation traces corresponding to **a–c**, respectively. Red lines, compressed pulse after phase correction; blue lines, uncompressed pulse; black lines, traces calculated by taking the spectra shown in **a–c** and assuming a flat spectral phase. Light grey traces show the range of simulated autocorrelation traces.

the individual frequencies from their ideal, evenly spaced positions. Such frequency shifts would give rise to phase errors for the different spectral lines that grow in time according to $\delta\varphi_n = 2\pi\delta f_n t$. As the $\delta f_n$, and hence the linear drifts of the $\delta\varphi_n$, are taken as uncorrelated, the characteristic size of the phase errors should (conservatively) satisfy $|\delta\varphi_n| < 0.7\pi$ to avoid significant waveform changes. With an observation time of 3,600 s, we may then estimate that the assumed $\delta f_n$ are conservatively of the order of $1 \times 10^{-4}$ Hz or below. Our estimation is consistent with measurements performed for combs from silica microtoroids by beating with a self-referenced comb from a mode-locked laser, indicating uniformity in the comb spacing at least at the $1 \times 10^{-3}$ Hz level[14].

In contrast to the data presented so far for type-I combs, for which the time-domain data indicate good coherence, we now discuss our observations for type-II combs, in which the initial sidebands are spaced by multiple FSRs from the pump. First we discuss the compression experiments for a type-II comb obtained from a 200-μm-radius ring pumped at ~1,549 nm, with the directly generated spectrum of Fig. 3d. We performed pulse compression experiments on a group of 24 comb lines centred at ~1,558 nm. The spectrum after smoothing and phase correction is shown in Fig. 6a, and the autocorrelation data are shown in Fig. 6d. Once again, phase compensation results in substantial compression compared to the original waveform, which shows only weak modulation. However, a new feature is that the on–off contrast of the experimental autocorrelation is significantly worse than the simulated trace, which assumes phases that are frequency-independent and constant in time. The significantly degraded autocorrelation contrast is a hallmark of partial coherence, which can occur when the spectral phase function varies in a non-trivial way during the measurement time.

It is known that the autocorrelation of continuous intensity noise consists of a single peak centred at zero delay on top of a constant positive background[36,37]. For a Gaussian random field with phases that are completely randomized, the ratio of the peak value to the background is 2:1. The width of the autocorrelation peak gives the timescale for the intensity fluctuations and does not imply the existence of a meaningful pulse duration. Furthermore, the shape of the autocorrelation will not be affected by spectral phase shaping. On the other hand, a coherent train of periodic pulses shows a series of peaks at delays corresponding to the pulse separation and exhibits high autocorrelation contrast. The autocorrelation trace does provide information on the pulse duration and may definitely be changed by spectral phase shaping. In our experiments with type-II combs, the autocorrelation shows contrast better than 2:1, but significantly less than would be expected with perfect phase compensation. The portion of the autocorrelation above the background remains responsive to spectral phase shaping and allows compression to bandwidth-limited peaks that repeat at the inverse of the comb spacing. This behaviour corresponds to fluctuations of the spectral phase on a timescale that is fast compared to the measurement time and with amplitude that is significant but less than $2\pi$—in other words, partial coherence. In this regime the signal consists of a deterministic average waveform superimposed with fluctuating noise-like waveforms with the same repetition period. As explained in the Supplementary Information, a rough estimate of the amplitude of the spectral phase fluctuations may be obtained from the autocorrelation contrast. From the data in Supplementary Fig. S1, we estimate uncorrelated variations of the spectral phase over an approximate range of $\pm 0.4\pi$.

We have observed similar autocorrelation data characteristic of partial coherence in a number of experiments with type-II combs, with minima of the experimental autocorrelation traces lying above the simulated ones assuming full coherence by 17–28% relative to the peak. The uncertainty in simulated traces

is estimated by repeating the simulations for 10–20 spectra recorded sequentially during the autocorrelation measurement. The simulated traces with largest positive and negative variation in contrast are shown as light grey lines in Fig. 6d; this variation is significantly less than that observed experimentally. In contrast, experimental autocorrelations for type-I combs exhibit minima that are, at most, 5% above simulated traces. This difference is sufficiently small that it may arise from a combination of effects such as uncertainty or variation in power spectra used for simulations, imperfect compensation of average spectral phase, and in some cases contributions from amplified spontaneous emission (ASE). Although we cannot rule out some level of fast phase fluctuations, our type-I combs clearly exhibit significantly lower phase fluctuations and higher coherence than type-II combs.

Figure 6e,f shows another interesting example obtained with 100-μm-radius rings (for directly generated spectra, see Fig. 3e,f). Here we pump a mode at ∼1,551.67 nm, which most readily generates stable comb spectra at a spacing of 460 GHz (twice the FSR). The spectrum after shaping and amplification comprises eight lines (as shown in Fig. 6b), and the experimental and simulated autocorrelation traces exhibit comparable contrast in Fig. 6e. Thus, the coherence of this comb appears to be high, similar to type-I combs. However, if the pump wavelength is tuned sufficiently while maintaining lock[38] to the same resonance, the spectrum broadens and intermediate comb lines fill in, resulting in a type-II comb with 230 GHz spacing. Directly generated and post-shaper spectra and the autocorrelation traces are shown in Figs 3f and 6c,f for pumping at ∼1,551.74 nm, a large shift compared to the low-power linewidth. Although the shapes of the compressed and simulated autocorrelation traces are similar, with a FWHM of 432 fs, the experimental background level is significantly increased, again indicating reduced coherence for type-II combs. This example demonstrates important coherence differences in combs generated from the same resonance in the same device under different pumping conditions.

In summary, we have demonstrated line-by-line pulse shaping on frequency combs generated from silicon nitride microring resonators. Combs formed via distinct routes (types I and II in the text) represent different time-domain behaviours corresponding to coherent and partially coherent properties. For type-I combs, nearly bandwidth-limited optical pulses were achieved after spectral phase correction, and a simple example of arbitrary waveform generation was presented. For type-II combs, compressed pulse trains were accompanied by significant autocorrelation background, signifying larger spectral phase fluctuations. The ability to controllably compress and reshape combs generated through nonlinear wave mixing in microresonators provides new evidence of phase coherence (or partial coherence) across the spectrum. Furthermore, in future investigations the ability to extract the phase of individual lines may furnish clues into the physics of the comb generation process.

## Methods

**Device fabrication.** We started with a (100) silicon wafer. A 3-μm-thick silicon dioxide layer was grown in a thermal oxidation furnace. A silicon nitride layer was then deposited using low-pressure chemical vapour deposition. The nitride layer was patterned with electron-beam lithography and etched through using a reactive ion etch (RIE) of $CHF_3/O_2$ to form microring resonators and waveguides coupling light into and out of the resonators. The waveguides were linearly tapered to a width of ∼100 nm at their end for low-loss coupling to and from optical fibres[39]. Another 3 μm oxide layer was deposited using a low temperature oxide furnace for the top cladding. The wafer was annealed for 3 h at 1,200 °C in an ambient $N_2$ environment. A photolithography and lift-off process was used to define a metal mask for V-grooves to provide self-aligned regions where the on-chip waveguide inverse tapers were accessible by optical fibres placed in the V-grooves. After mask definition, the V-grooves were formed by RIE of the unprotected oxide and nitride layers and KOH etching of the silicon. The height of the ring resonators was 430 nm and 550 nm for devices corresponding to Fig. 3a and Fig. 3b–f, respectively. The widths of the rings and of the accessing waveguides were 2 μm and 1 μm throughout. The radii indicated in the text are those at the outermost edge of the devices. The gap between the ring and the waveguide was 700 nm in Fig. 3a, 500 nm in Fig. 3b, and 800 nm in Fig. 3c–f. The difference in ring–waveguide gap has the effect of modifying the device coupling.

**Experimental procedure.** Microresonators were pumped with c.w. powers (estimated to be between 66 mW and 1.4 W) coupled into the input guide, and in all cases were well above the threshold for comb formation. Line-by-line pulse shaping was implemented using a fibre-coupled Fourier-transform pulse shaper that incorporated a 2 × 128 pixel liquid-crystal modulator array to independently control both the intensity and phase of each spectral line. The output waveform from the pulse shaper was fed to an intensity autocorrelation set-up through an EDFA. The path from the output of the microring chip to the autocorrelator comprised ∼18 m of standard single-mode fibre. The thickness of the β-barium borate crystal used for SHG was 0.6 mm, corresponding to an estimated 1 dB phase-matching bandwidth of 200 nm, well beyond the bandwidth of the combs investigated here. Briefly, the phase was corrected by adjusting the phase of one comb line at a time to maximize the SHG signal from the autocorrelation measurement at zero delay. To optimize the SHG signal, the phase of the new frequency component was varied from 0 to $2\pi$ in steps of $\pi/12$. Once the SHG was optimized, the pulses were compressed close to the bandwidth limit, and the opposite of the phase applied on the pulse shaper gave an estimate of the original spectral phase after the comb had propagated to the autocorrelator.

Received 17 March 2011; accepted 8 September 2011; published online 9 October 2011

## References


1. Udem, T., Holzwarth, R. & Hänsch, T. W. Optical frequency metrology. *Nature* **416,** 233–237 (2002).
2. Diddams, S. A., Bergquist, J. C., Jefferts, S. R. & Oates, C. W. Standards of time and frequency at the outset of the 21st century. *Science* **306,** 1318–1324 (2004).
3. Keilmann, F., Gohle, C. & Holzwarth, R. Time-domain mid-infrared frequency-comb spectrometer. *Opt. Lett.* **29,** 1542–1544 (2004).
4. Schliesser, A., Brehm, M., Keilmann, F. & Weide van der, D. W. Frequency-comb infrared spectrometer for rapid, remote chemical sensing. *Opt. Express* **13,** 9029–9038 (2005).
5. Diddams, S. A., Hollberg, L. & Mbele, V. Molecular fingerprinting with the resolved modes of a femtosecond laser frequency comb. *Nature* **445,** 627–630 (2007).
6. Thorpe, M. J., Moll, K. D., Jones, J. J., Safdi, B. & Ye, J. Broadband cavity ringdown spectroscopy for sensitive and rapid molecular detection. *Science* **311,** 1595–1599 (2006).
7. Coddington, I., Swann, W. C. & Newbury, N. R. Coherent multiheterodyne spectroscopy using stabilized optical frequency combs. *Phys. Rev. Lett.* **100,** 013902 (2008).
8. Jones, D. J. *et al.* Carrier-envelope phase control of femtosecond mode-locked lasers and direct optical frequency synthesis. *Science* **288,** 635–639 (2000).
9. Murata, H., Morimoto, A., Kobayashi, T. & Yamamoto, S. Optical pulse generation by electrooptic-modulation method and its application to integrated ultrashort pulse generators. *IEEE J. Sel. Top. Quantum Electron.* **6,** 1325–1331 (2000).
10. Yamamoto, T., Komukai, T., Suzuki, K. & Takada, A. Spectrally flattened phase-locked multi-carrier light generator with phase modulators and chirped fibre Bragg grating. *Electron. Lett.* **43,** 1040–1042 (2007).
11. Wu, R., Supradeepa, V. R., Long, C. M., Leaird, D. E. & Weiner, A. M. Generation of very flat optical frequency combs from continuous-wave lasers using cascaded intensity and phase modulators driven by tailored radio frequency waveforms. *Opt. Lett.* **35,** 3234–3226 (2010).
12. Kourogi, M., Nakagawa, K. & Ohtsu, M. Wide-span optical frequency comb generator for accurate optical frequency difference measurement. *IEEE J. Quantum Electron.* **29,** 2693–2701 (1993).
13. Kippenberg, T. J., Holzwarth, R. & Diddams, S. A. Microresonator-based optical frequency combs. *Science* **332,** 555–559 (2011).
14. DelHaye, P. *et al.* Optical frequency comb generation from a monolithic microresonator. *Nature* **450,** 1214–1217 (2007).
15. Levy, J. S. *et al.* CMOS-compatible multiple-wavelength oscillator for on-chip optical interconnects. *Nature Photon.* **4,** 37–40 (2010).
16. Razzari, L. *et al.* CMOS compatible integrated optical hyper-parametric oscillator. *Nature Photon.* **4,** 41–45 (2010).
17. Grudinin, I. S., Yu, N. & Maleki, L. Generation of optical frequency combs with a $CaF_2$ resonator. *Opt. Lett.* **34,** 878–880 (2009).
18. DelHaye, P., Arcizet, O., Schliesser, A., Holzwarth, R. & Kippenberg, T. J. Full stabilization of a microresonator-based optical frequency comb. *Phys. Rev. Lett.* **101,** 053903 (2008).
19. Del'Haye, P. *et al.* Octave spanning tunable frequency comb from a microresonator. *Phys. Rev. Lett.* **107,** 063901 (2011).
20. Foster, M. A. *et al.* Silicon-based monolithic optical frequency comb source. *Opt. Express* **19,** 14233–14239 (2011).

21. Okawachi, Y. *et al.* Octave-spanning frequency comb generation in a silicon nitride chip. *Opt. Lett.* **36,** 3398–3400 (2011).
22. Ferrera, M. *et al.* Low power four wave mixing in an integrated, micro-ring resonator with $Q = 1.2$ million. *Opt. Express* **17,** 14098–14103 (2009).
23. Arcizet, O., Schliesser, A., Del'Haye, P., Holzwarth, R. & Kippenberg, T. J. Optical frequency comb generation in monolithic microresonators, in *Practical Applications of Microresonators in Optics and Photonics* (Taylor & Francis, 2009).
24. Weiner, A. M. Femtosecond pulse shaping using spatial light modulators. *Rev. Sci. Instrum.* **71,** 1929–1960 (2000).
25. Jiang, Z., Seo, D. S., Leaird, D. E. & Weiner, A. M. Spectral line by line pulse shaping. *Opt. Lett.* **30,** 1557–1559 (2005).
26. Miyamoto, D. *et al.* Waveform-controllable optical pulse generation using an optical pulse synthesizer. *IEEE Photon. Technol. Lett.* **18,** 721–723 (2006).
27. Jiang, Z., Huang, C.-B., Leaird, D. E. & Weiner, A. M. Optical arbitrary waveform processing of more than 100 spectral comb lines. *Nature Photon.* **1,** 463–467 (2007).
28. Fontaine, N. K. *et al.* 32 phase × 32 amplitude optical arbitrary waveform generation. *Opt. Lett.* **32,** 865–867 (2007).
29. Cundiff, S. T. & Weiner, A. M. Optical arbitrary waveform generation. *Nature Photon.* **4,** 760–766 (2010).
30. Huang, C. B., Park, S. G., Leaird, D. E. & Weiner, A. M. Nonlinearly broadened phase-modulated continuous-wave laser frequency combs characterized using DPSK decoding. *Opt. Express* **16,** 2520–2527 (2008).
31. Miao, H., Leaird, D. E., Langrock, C., Fejer, M. M. & Weiner, A. M. Optical arbitrary waveform characterization via dual-quadrature spectral shearing interferometry. *Opt. Express* **17,** 3381–3389 (2009).
32. Chembo, Y. K., Strekalov, D. V. & Yu, N. Spectrum and dynamics of optical frequency combs generated with monolithic whispering gallery mode resonators. *Phys. Rev. Lett.* **104,** 103902 (2010).
33. Agha, I. H., Okawachi, Y. & Gaeta, A. L. Theoretical and experimental investigation of broadband cascaded four-wave mixing in high-Q microspheres. *Opt. Express* **17,** 16209–16215 (2009).
34. Papp, S. B. & Diddams, S. A. Spectral and temporal characterization of a fused-quartz microresonator optical frequency comb. Preprint at http://arxiv.org/abs/1106.2487v1 (2011).
35. Heritage, J. P., Weiner, A. M. & Thurston, R. N. Picosecond pulse shaping by spectral phase and amplitude manipulation. *Opt. Lett.* **10,** 609–611 (1985).
36. Ippen, E. P. & Shank, C. V. *Ultrashort Light Pulses* (Springer-Verlag, 1977).
37. Weiner, A. M. *Ultrafast Optics* (John Wiley & Sons, 2009).
38. Carmon, T., Yang, L. & Vahala, K. J. Dynamic thermal behavior and thermal self-stability of microcavities. *Opt. Express* **12,** 4742–4750 (2004).
39. Shoji, T., Tsuchizawa, T., Watanabe, T., Yamada, K. & Morita, H. Low loss mode size converter from 0.3 μm square Si wire waveguides to single mode fibres. *Electron. Lett.* **38,** 1669–1670 (2002).


## Acknowledgements

The authors gratefully acknowledge the comments and suggestions from V. Aksyuk, M. Qi, C. Long and Victor Torres Company, and thank the staff of the CNST Nanofab, particularly R. Kasica, for assistance with electron-beam lithography. This project was supported in part by the National Science Foundation (grants ECCS-0925759 and ECCS-1102110), by the Naval Postgraduate School (grant N00244-09-1-0068) under the National Security Science and Engineering Faculty Fellowship programme, and by the NIST-CNST/UMD-NanoCenter Cooperative Agreement. Any opinions, findings and conclusions or recommendations expressed in this publication are those of the authors and do not necessarily reflect the views of the sponsors.

## Author contributions

F.F. led the pulse-shaping and compression experiments, with assistance from D.E.L., H.M. and J.W. H.M. led device fabrication with the assistance of L.C. Microring design and/or characterization was carried out by F.F., K.S. and L.T.V. The project was organized and coordinated by A.M.W. and H.M. A.M.W., H.M., F.F., D.E.L. and K.S. contributed to the writing.

## Additional information

The authors declare no competing financial interests. Supplementary information accompanies this paper at www.nature.com/naturephotonics. Reprints and permission information is available online at http://www.nature.com/reprints. Correspondence and requests for materials should be addressed to H.M. and A.M.W.